Demonstration of the rotational viscosity transfer across scales in Navier–Stokes turbulence

Satori Tsuzuki*

Research Center for Advanced Science and Technology,
University of Tokyo, 4-6-1, Komaba, Meguro-ku, Tokyo 153-8904, Japan

Mechanical effects that span multiple physical scales—such as the influence of vanishing molecular viscosity on large-scale flow structures under specific conditions—play a critical role in real fluid systems. The spin angular momentum-conserving Navier–Stokes equations offer a theoretical framework for describing such multiscale fluid dynamics by decomposing total angular momentum into bulk and intrinsic spin components. However, this framework still assumes locally non-solid rotational flows, a condition that remains empirically unverified. This study addresses such unvalidated assumptions intrinsic to the model and extends it within the framework of turbulence hierarchy theory. The theory suggests that under certain conditions, small-scale structures may transfer to larger scales through the rotational viscosity. To verify this, we conducted spectral analyses of freely decaying two-dimensional turbulence initialized with a vortex-concentrated distribution. The results indicate that rotational viscosity exhibits interscale transfer behavior, revealing a new mechanism by which order can propagate from small to large scales in Navier–Stokes turbulence.

I. INTRODUCTION

Turbulence exhibits intricate hierarchical and ordered structures, posing a longstanding challenge in fluid dynamics. A fundamental understanding of these features has been pursued from both statistical-mechanics and dynamics perspectives. Milestones in the statistical-mechanics approach include Onsager's prediction of inverse energy cascades in two-dimensional (2D) turbulence and Kraichnan's spectral theory, both of which provided insights into energy transfer mechanisms [1–4]. Multiscale dynamics—including microscopic phenomena influencing macroscopic flow structures—play a critical role in real fluid systems. A prominent example is found in macroscopic quantum fluids [5, 6], where the near-zero molecular viscosity at cryogenic temperatures enables the formation of quantum vortices with minimal dissipation. These quantum-scale features can, in turn, affect large-scale dynamics, giving rise to striking behaviors such as the fountain effect and film flow. Such phenomena underscore the need for a multiscale fluid dynamical model that can consistently account for interactions across disparate physical scales. One promising candidate is the spin-angular-momentum-conserving Navier–Stokes model, originally proposed in 1964 [7, 8]. This extended formulation provides a framework for describing multiscale fluid dynamics bridging classical and quantum regimes. The model distinctly separates the local total angular momentum into two components: the contribution from the bulk fluid and the internal spin degrees of freedom associated with the constituent particles, such as molecules. This decomposition permits the inclusion of internal rotational motion—specifically, particle-scale angular velocity—into the continuum-level equations of motion. While mathematically consistent with the conventional Navier–Stokes equations, this formulation is particularly well-suited for systems in which internal rotation affects macroscopic behavior. Applications include polar fluids [9], complex suspensions [10], and other structured media where microscopic rotation is non-negligible. More recently, it has been suggested that this model possesses a mathematical structure capable of mediating inter-scale coupling, allowing microscale interactions (such as among small-scale vortices) to influence macroscale flow features, as discussed in section 3.2 of Ref. [11]. This potential has renewed interest in the model as a candidate framework for multiscale fluid dynamics.

However, this formulation assumes that local rotational motion can be non-solid, meaning the spinning of constituent fluid particles does not always coincide with solid body rotation. Specifically, when the local fluid velocity is denoted by $\mathbf{u}$, the vorticity by $\boldsymbol{\omega}$, and the angular velocity by $\boldsymbol{\omega}_0$, the model assumes that $\boldsymbol{\omega}$ is not always equal to $2\boldsymbol{\omega}_0$. This assumption is uncommon in classical fluid mechanics because the local nature of fluid particles usually ensures solid rotational flow at every point. Verifying this assumption is challenging, as it requires understanding the relationship between vortex stretching and tilting geometric features [12] and the deformation of fluid particles. Furthermore, in 2D problems where vortex stretching and tilting are absent, a theoretical justification of the assumption is necessary before the model can be confidently applied.

This study addresses this open question by developing a continuum-mechanical derivation of the

* Email: tsuzukisatori@g.ecc.u-tokyo.ac.jp

$\boldsymbol{\omega} = \nabla \times \mathbf{u} \neq 2\boldsymbol{\omega}_0$ condition in 2D, and by exploring its validity through numerical simulations. Specifically, we examine a freely decaying 2D turbulent flow initialized with a set of point vortices exhibiting localized circulation. This configuration mimics the state of a system immediately following the release of externally controlled condition—for example, in phase-modulated polar or quantum fluids. Our analysis shows that the quantity $\boldsymbol{\omega} - 2\boldsymbol{\omega}_0$ is directly proportional to the first-order spatial displacement, making it non-negligible under specific conditions. In addition, the spin angular momentum conserving Navier–Stokes equations, when extended to a multiscale physics framework, theoretically suggest that rotational viscosity can be transferred to larger scales under particular conditions. This study investigates the particular conditions under which local non-solid rotational flow occurs and proposes that rotational viscosity can be transferred between scales in a system with a concentrated point vortex and circulation. To verify this, spectral analyses were conducted on freely decaying 2D turbulence that was initialized with a distribution of concentrated vortices. The results show that rotational viscosity exhibits interscale transfer behavior, revealing a novel mechanism by which order can propagate from small to large scales in Navier–Stokes turbulence.

II. GOVERNING EQUATIONS OF MULTISCALE FLUID MECHANICS

Model overview.—The Navier–Stokes equation incorporating spin angular momentum conservation was derived by D.W. Condiff in 1964 through the following procedure. First, the local total angular momentum $\mathbf{M}$ is decomposed into two parts: the angular momentum of the bulk fluid ($\mathbf{r} \times \mathbf{u}$) and the internal degrees of freedom of the constituent particles ($\mathbf{l}$) as $\mathbf{M} = \mathbf{r} \times \mathbf{u} + \mathbf{I}$. The vector $\mathbf{I}$ is the spin angular momentum intrinsic to each constituent particle. Vectors $\mathbf{r}$ and $\mathbf{u}$ represent the coordinates and velocity of the local fluid fragment, respectively. Vector $\mathbf{I}$ can be further expressed as the product of the moment of inertia of the constituent particles and the spin field defined on the constituent particles as $\mathbf{I} = \bar{\mathbf{I}} \cdot \boldsymbol{\omega}_0$ where $\bar{\mathbf{I}}$ is the tensor field, expressed as a scalar multiple of the unit dyadic $\mathbf{U}$ as $\bar{\mathbf{I}} = I\mathbf{U}$ and thereby $\bar{\mathbf{I}} \cdot \boldsymbol{\omega}_0 = I\mathbf{U}\boldsymbol{\omega}_0 = I\boldsymbol{\omega}_0$, where $\boldsymbol{\omega}_0$ is now represented as a vector. This relation assumes a uniform and isotropic spin field for each constituent particle. In this case, $\boldsymbol{\omega}_0$ represents the angular velocity vector around the axis of the constituent particle.

Substituting these relations ($\mathbf{M} = \mathbf{r} \times \mathbf{u} + \mathbf{I}$ and $\mathbf{I} = I\boldsymbol{\omega}_0$) and the following assumptions into the three equations: a) Cauchy's equation of motion,

b) the conservation law for the local angular momentum $\mathbf{M}$ derived from Reynolds' transport theorem, and c) the evolution equation for the spin angular momentum $\mathbf{I}$ derived from these equations, we obtain the spin-angular-momentum conserving Navier–Stokes equation. The two assumptions mentioned above are as follows: (1) Newtonian fluid assumption—This allows us to divide the stress tensor $\mathbf{T}$ into a symmetric part $\mathbf{T}_s$ and an asymmetric part $\mathbf{T}_a$ of the stress tensor, where $\mathbf{T}_s$ is proportional to the symmetrized velocity gradient tensor. The couple stress tensor is assumed to depend only on the symmetrized spin gradient tensor. (2) Possibility of non-solid rotation of fluid particles—If the local vorticity is $\boldsymbol{\omega} = \nabla \times \mathbf{u}$ and the angular velocity of the constituent particles at that location is $\boldsymbol{\omega}_0$ and the deviation from the solid rotating flow contributes to the asymmetric part of the stress tensor: $\mathbf{T}_a = \eta_r(\boldsymbol{\omega} - 2\boldsymbol{\omega}_0)$. The resulting hydrodynamic equation is described as follows:

$$
\begin{aligned}
\frac{D\mathbf{u}}{Dt} = & -\frac{1}{\rho}\nabla P + (\eta + \eta_r)\nabla^2 \mathbf{u} \\
& + \left(\frac{\eta}{3} + \xi - \eta_r\right)\nabla\nabla \cdot \mathbf{u} \\
& + 2\eta_r \nabla \times \boldsymbol{\omega}_0 + \mathbf{F}, \quad (1)
\end{aligned}
$$

where $D\{\cdot\}/Dt$ is the material derivative. P is pressure. $\mathbf{u}$ denotes the velocity of a constituent particle, and $\boldsymbol{\omega}_0$ represents the angular velocity of the particle around its axis. $\mathbf{F}$ is an external force. The parameter η signifies the shear viscosity, ξ indicates the bulk viscosity, and η_r represents the rotational viscosity coefficients, respectively. A detailed step-by-step derivation of Eq. (1) is presented in Fig. 9 of Ref. [13] in a tabular format.

The resulting Eq. (1) represents an extension of the conventional Navier–Stokes equation. When the rotational viscosity η_r is set close to zero, the fourth term on the right-hand side vanishes. In this case, only the shear viscosity in the first term and the shear and bulk viscosities in the second term on the right-hand side remain. As a result, Eq. (1) reduces to the usual compressible Navier–Stokes equations. Furthermore, since this study focuses only on incompressible fluids, the incompressibility condition $\nabla \cdot 0$ always holds, implying that the third term on the right-hand side becomes zero. Therefore, the only distinctive feature of Eq. (1) compared to the usual Navier–Stokes equation is the rotation term in the fourth term on the right-hand side.

The angular velocity $\boldsymbol{\omega}_0$ was originally introduced not as a characteristic of fluid constituents (i.e., fluid particles), but as a molecular-scale variable. Specifically, the local angular momentum $\mathbf{M}$ is decomposed into the angular momentum of the bulk flow, $\boldsymbol{r} \times \boldsymbol{u}$, and the internal degrees of freedom (e.g.,

spin) of individual molecules. However, this interpretation is inconsistent with classical fluid mechanics, wherein molecules are regarded as infinitesimal, and no deformation is assumed at a point. Consequently, molecular-level rotation is treated such that $\boldsymbol{\omega} = 2\boldsymbol{\omega}_0$. Unfortunately, interpreting $\boldsymbol{\omega}_0$ as a fluid particle variable also contradicts classical fluid mechanics in a strict sense. Fluid particles (or fluid percels) are typically defined as small virtual element with a characteristic size that is smaller than the Kolmogorov scale, which is the minimum scale of an eddy, but is much larger than the free paths of molecules [14–16]. Under this assumption, local rotational flow within a fluid particle is considered solid-body rotation, implying that $\boldsymbol{\omega} = 2\boldsymbol{\omega}_0$ always holds. As a result, $\mathbf{T}_a = \eta_r(\boldsymbol{\omega} - 2\boldsymbol{\omega}_0)$ vanishes, rendering Eq. (1) physically irrelevant. The case of compressible fluids is no exception—while bulk deformation may occur, deformation of fluid particles, being sufficiently small compared to the macroscopic length scale, is rarely considered. However, in mesoscale dynamics such as molecular dynamics or dissipative particle dynamics (DPD) [17–19], fluid particles are interpreted as coarse-grained entities [20–22] representing groups of atoms or molecules, which can undergo deformation. In such frameworks, local vortex stretching and tilting can be defined at the level of fluid particles, and the deviation between $\boldsymbol{\omega}$ and $2\boldsymbol{\omega}_0$ naturally contributes to the antisymmetric part of the stress tensor. Under these conditions, Eq. (1) becomes valid. This empirical justification supports the use of $\boldsymbol{\omega}_0$ as a fluid-particle variable in mesoscale dynamics.

Nevertheless, interpreting $\boldsymbol{\omega}_0$ as a variable defined on coarse-grained particles that represent atoms or molecules introduces a challenge: establishing a relationship between $\boldsymbol{\omega}_0$ and the actual microscopic rotational behavior of molecules. In other words, the material properties associated with $\boldsymbol{\omega}_0$ must be well defined. Establishing a quantitative relationship between $\boldsymbol{\omega}$—a continuum scale variable—and the microscopic parameters of atoms and molecules is far from trivial. Although the derivation of Eq. (1) is accompanied by a time-evolution equation for variable $\boldsymbol{\omega}_0$ (see Eq. (13) in Ref. [7] if needed), this equation cannot be solved deterministically for several real cases due to the lack of an initial condition for $\boldsymbol{\omega}_0$. Put simply, the system of equations is underdetermined by one equation governing $\boldsymbol{\omega}_0$. For these reasons, Eq. (1) has been largely limited to applications in chemical engineering and related fields.

Spin-field correspondence.—A critical issue is that $\boldsymbol{\omega}_0$ is defined only "on" individual particles and not as a field variable. This leads to a problem when applying the relation $\mathbf{T}_a = \eta_r(\boldsymbol{\omega} - 2\boldsymbol{\omega}_0)$ at the particle scale, as it becomes meaningless if $\boldsymbol{\omega} = 2\boldsymbol{\omega}_0$. Al-

ternatively, if the relation holds over a larger region, the continuity condition for $\boldsymbol{\omega}_0$ is not preserved at the particle scale.

A recent proposal in Ref. [11] offers a viable solution to this inconsistency. The underlying concept involves substituting the spin variable $\boldsymbol{\omega}_0$ with a field variable $\overline{\boldsymbol{\varpi}}$. This approach is grounded in the notion that the fundamental fluid unit can be characterized as a field, rather than a particle. This perspective shares similarities with the turbulence hierarchy, which effectively decomposes turbulence into distinct eddy structures. A constitutive relationship is then established between $\overline{\boldsymbol{\varpi}}$ and $\boldsymbol{\omega}_0$, thereby reconciling the local and nonlocal viewpoints.

$$\overline{\boldsymbol{\varpi}}(\mathbf{r}) := \frac{1}{C} \int \frac{\boldsymbol{\omega}_0(\mathbf{r}')}{|\mathbf{r} - \mathbf{r}'|} \, d\mathbf{r}', \qquad (2)$$

where C is a constant coefficient. The transformation between $\boldsymbol{\omega}_0$ and $\overline{\boldsymbol{\varpi}}$ as defined by Eq. (2) can be expressed as $\overline{\boldsymbol{\varpi}} = \mathcal{F}[\boldsymbol{\omega}_0]$, where $\mathcal{F}[\cdot]$ denotes the convolution integral operator on the right-hand side of Eq. (2). The internal inconsistency in Eq. (1), which requires $\boldsymbol{\omega} = 2\boldsymbol{\omega}_0$ at each fluid particle even if $\boldsymbol{\omega} \neq 2\boldsymbol{\omega}_0$, can be resolved by reinterpreting Eq. (2) within the framework of hierarchical concept of turbulence theory. Specifically, Eq. (2) may be understood as defining a scale transformation from small-scale vortices characterized by $\boldsymbol{\omega}_0$ to large-scale vortices represented by $\overline{\boldsymbol{\varpi}}$, mediated by the operator $\mathcal{F}[\cdot]$. From a large-scale perspective, the motion of a small-scale vortex is sufficiently localized to be considered as localized solid-body rotation. Consequently, we acknowledge that the difference between $\boldsymbol{\omega}$ and $2\boldsymbol{\omega}_0$ may be nonzero when examining the small-scale vortices from the same level, while the small scale vorticity can still be approximated as $\boldsymbol{\omega} = 2\boldsymbol{\omega}_0$ when viewed from a large-scale perspective. Therefore, $\boldsymbol{\omega}_0$ on the right-hand side can be considered as $(1/2)\boldsymbol{\omega}$, as acknowledged in classical fluid mechanics, and this relation holds across scales. Then, vorticity $\overline{\boldsymbol{\varpi}}$ at a large-scale is obtained from the convolution integral of the vortices characterized by $\boldsymbol{\omega} \, (= 2\boldsymbol{\omega}_0)$ at its subscale. Notably, Eq. (2) only states that the vorticity at a given scale is obtained from the vorticity distribution at a finer subscale, without implying any discontinuity in the fluid; no singularities exist at position $\mathbf{r}$.

The relationship between $\boldsymbol{\omega}_0$ and $\overline{\boldsymbol{\varpi}}$ is analogous to the relationship in electromagnetism between the steady current density $\mathbf{i}$, the resulting magnetic field $\mathbf{B}$, and the vector potential $\mathbf{A}$ satisfying $\mathbf{B} = \nabla \times \mathbf{A}$. In fact, $\overline{\boldsymbol{\varpi}}$ plays the role of a rotational potential induced by the spatial distribution of the local angular velocity $\boldsymbol{\omega}_0$ of fluid particles. The curl $\nabla \times \overline{\boldsymbol{\varpi}}$ thus represents the rotational force induced at position $\mathbf{r}$, which can be interpreted as a form of viscosity.

Specifically, $\nabla \times \boldsymbol{\omega} = \nabla \times (\nabla \times \mathbf{u}) = \nabla(\nabla \cdot \mathbf{u}) - \nabla^2 \mathbf{u} = -\nabla^2 \mathbf{u}$, where we have used the incompressibility condition $\nabla \cdot \mathbf{u} = 0$. Hence, $\nabla \times \boldsymbol{\omega}$ effectively conveys the rotational viscosity.

Replacing $\boldsymbol{\omega}_0$ with $\overline{\boldsymbol{\omega}}$ in the derivation of Eq. (1) and substituting $(1/2)\boldsymbol{\omega}$ into Eq. (2), the rotational contribution in Eq. (1) can be further reformulated as follows using simple vector relations:

$$\nabla \times \overline{\boldsymbol{\omega}}(\mathbf{r}) = \left(\frac{1}{2C}\right)\int \frac{\boldsymbol{\omega}(\mathbf{r}') \times (\mathbf{r} - \mathbf{r}')}{|\mathbf{r} - \mathbf{r}'|^3}\, d\mathbf{r}' + \mathcal{F}\Big[\nabla \times \boldsymbol{\omega}(\mathbf{r})\Big]. \quad (3)$$

Denote the hierarchical depth level of vortex structures by an index n, such that large-scale vortices are associated with depth n, and subgrid-scale vortices correspond to depth $n+1$. In Eq. (3), the left-hand side represents the vorticity at depth n, while the first term on the right-hand side represents vortex–vortex interactions at depth $n+1$. The second term on the right-hand side corresponds to the rotational field $\nabla \times \boldsymbol{\omega}$ at depth $n+1$, filtered through the operator $\mathcal{F}$. Notably, Eq. (3) can be expressed as a recursive relation of the form $\mathbf{X}^{(n)} = \mathbf{Y}^{(n+1)} + \mathcal{F}[\mathbf{X}^{(n+1)}]$, where $\mathbf{X} = \nabla \times \boldsymbol{\omega}$, and $\mathbf{Y}$ denotes the vortex interaction term at depth $n+1$. Within this hierarchical framework, a generalized form of Eq. (3) from depth n to k can be written as

$$\mathbf{X}^{(n)} = \mathbf{Y}^{(n+1)} + \mathcal{F}\Big(\mathbf{Y}^{(n+2)} + \mathcal{F}\Big(\mathbf{Y}^{(n+3)} + \cdots + \mathcal{F}\Big[\mathbf{X}^{(n+k)}\Big]\Big)\Big). \quad (4)$$

Let us now consider a case in which the subgrid scale reaches the Kolmogorov minimum scale, but the vortex remains stable. A representative example is the quantum vortex in liquid helium-4 cooled to cryogenic temperatures. Since no smaller vortices exist, the second term on the right-hand side of Eq. (3) is zero. On the other hand, the vorticity $\boldsymbol{\omega}$ is localized on the vortex filaments and thus is expressed as

$$\boldsymbol{\omega}(\mathbf{r}) = \kappa \int_{\Gamma} \mathbf{s}'(\chi)\delta(\mathbf{r} - \mathbf{s}(\chi))\, d\chi, \quad (5)$$

where χ is the arc length along the vortex filaments, and s is the position vector from the origin to point χ on the filaments [23, 24]. The line integral Γ is taken along the vortex filaments, and κ denotes the intensity of circulation. The vectors $\mathbf{s}'$ and $\mathbf{s}''$ are defined such that $\mathbf{s}'$ is the tangent vector at point χ, and $\mathbf{s}''$ is the vector perpendicular to $\mathbf{s}'$. Additionally, $\mathbf{s}'$, $\mathbf{s}''$, and the cross product $(\mathbf{s}' \times \mathbf{s}'')$ are mutually orthogonal. The partial derivatives of $\mathbf{s}$ with respect to χ are given by $\frac{\partial \mathbf{s}}{\partial \chi} = \mathbf{s}'$. After applying the condition that the second term on the right-hand side of Eq. (3) is zero, we substitute Eq. (5) into Eq. (3) to obtain the relationship between the smallest-scale vortex and the vortex at the next scale.

$$\nabla \times \overline{\boldsymbol{\omega}}(\mathbf{r}) = \left(\frac{\kappa}{2C}\right)\int_{\Gamma} \frac{\mathbf{s}'(\chi) \times (\mathbf{r} - \mathbf{s}(\chi))}{|\mathbf{r} - \mathbf{s}(\chi)|^3}\, d\chi. \quad (6)$$

The right-hand side of Eq. (6) represents vortex-vortex interactions within a point vortex system comprising multiple vortices. This corresponds to a special case in which vortices do not dissipate at the smallest scale. The rotational forcing at this minimal scale, as expressed on the right-hand side of Eq. (6), is transmitted to larger scales through a recursive nesting structure—mathematically, a composition of recursive transformations—as described in Eqs. (3) or (4), ultimately reaching the large-scale regime via the rotational term in Eq. (1). In summary, by redefining the spin variable, originally defined only on discrete particles (fluid elements or molecules) in Eq. (1), as a continuous field variable through Eq. (2), we have demonstrated that the spin-angular-momentum-conserving Navier–Stokes equation inherently includes a mechanism for transferring vortex dynamics from small to large scales. In practical systems with significant dissipation, the dissipation effects of the scale transformation governed by the filtering function $\mathcal{F}$ alone may not be sufficient. Nonetheless, the underlying principle remains valid. In such cases, it is sufficient to reinterpret Eq. (4) as incorporating a composite filtering operation, $\mathcal{F} \circ \mathcal{G}$, where another filtering function $\mathcal{G}$ accounts for enhanced dissipation or scale-localized attenuation.

III. RETHINKING THE NON-SOLID ROTATIVITY

In continuum mechanics, the velocity gradient tensor $\nabla\mathbf{u}$ can be decomposed into the rate-of-strain tensor $\mathbf{E}$ and the rate-of-rotation tensor $\boldsymbol{\Omega}$ as follows:

$$\nabla\mathbf{u} = \mathbf{E} + \boldsymbol{\Omega}. \quad (7)$$

Here, $\mathbf{E}$ is a symmetric tensor satisfying $\mathbf{E}^{\mathsf{T}} = \mathbf{E}$, while $\boldsymbol{\Omega}$ is an antisymmetric tensor satisfying $\boldsymbol{\Omega}^{\mathsf{T}} = -\boldsymbol{\Omega}$. Now, consider a reference point $\mathbf{x}_0$, the velocity field $\mathbf{u}$ in the vicinity of $\mathbf{x}_0$ can be expanded in a Taylor series up to third order, retaining the residual terms, as follows:

$$\mathbf{u} = \mathbf{u}_0 + \nabla\mathbf{u} \cdot \Delta\mathbf{x} + \frac{1}{2}\frac{\partial^2 u_m}{\partial x_j \partial x_k}\Delta x_j \Delta x_k + R_m^{(3)}. \quad (8)$$

For notational convenience, higher-order terms beyond the first order are expressed in tensor form for each velocity component u_m $(m = 1, 2, 3)$. We have introduced Levi–Civita symbol and Einstein's summation convention. We define the position offset as $\Delta\mathbf{x} := \mathbf{x} - \mathbf{x}_0 = (\Delta x_1, \Delta x_2, \Delta x_3)$, and $R_m^{(3)}$ denotes the third-order residual term associated with the m-th component of the velocity. $\nabla \times \mathbf{u}_0 = 0$ because $\mathbf{u}_0$ is a constant vector. Substituting $\nabla\mathbf{u} = \mathbf{E} + \mathbf{\Omega}$ into Eq. (8), and applying standard vector and tensor calculus, we find that the contribution from the symmetric tensor $\mathbf{E}$ vanishes due to its self-cancellation under symmetry, leading to the following:

$$\nabla \times \mathbf{u} = 2\mathbf{\Omega} + \varepsilon_{inm}\frac{\partial^2 u_m}{\partial x_j \partial x_n}\Delta x_j + \tilde{R}_m^{(3)}, \qquad (9)$$

where $\tilde{R}_m^{(3)}$ represents the rotation of $R_m^{(3)}$ for m-th component of velocity. Here, we used the identity $\nabla \times (\mathbf{A} \cdot \mathbf{b}) = -(\mathbf{A}^\mathsf{T} - \mathbf{A})$ for tensor $\mathbf{A}$ and vector $\mathbf{b}$, where $\mathbf{A} = \mathbf{E} + \mathbf{\Omega}$ and $\mathbf{b} = \Delta\mathbf{x}$ in our case. The angular velocity vector $\boldsymbol{\omega}_0$ and the antisymmetric tensor $\mathbf{\Omega}$ are related by equation $\omega_k^{(0)} = \epsilon_{ijk}\Omega_{ij}$, where the lower subscript 0 is shifted to the upper subscript in component expression. In the context of rotational transformations, $\mathbf{\Omega}$ can be considered a vector of reduced dimensionality, and it is reasonable to equate $\mathbf{\Omega}$ with the angular velocity vector $\boldsymbol{\omega}_0$ $(\mathbf{\Omega} \equiv \boldsymbol{\omega}_0)$.

An important point to note here is that, although the third term on the right-hand side of Eq. (8) is proportional to the square of the infinitesimal displacement Δx_a $(a = i, j, \text{or } k)$, the second term on the right-hand side of Eq. (9), after the curl operation is applied, becomes linearly proportional to Δx_a. Therefore, the difference between the left-hand side and the first term on the right-hand side $\boldsymbol{\omega} - 2\boldsymbol{\omega}_0$ is directly proportional to Δx_a and is not negligible in most cases. Consequently, it is physically meaningful to incorporate the deviation from solid-body rotation into the antisymmetric part of the stress tensor $\mathbf{T}_a$, which can be achieved by defining $\mathbf{T}_a$ as $\mathbf{T}_a = \eta_r(\boldsymbol{\omega} - 2\boldsymbol{\omega}_0)$, where η_r is the rotational viscosity coefficient.

Through the rotation operation, the order of dependence on Δx_a in each term of Eq. (9) is reduced. Specifically, the second term becomes linearly proportional to the infinitesimal vector Δx_a, while the residual term $\tilde{R}_m^{(3)}$ depends at least on the square of Δx_a. Neglecting the residual term, the relation $\boldsymbol{\omega} - 2\mathbf{\Omega}$ becomes equal to the second term. Therefore, the non-vanishing nature of $\boldsymbol{\omega} - 2\mathbf{\Omega}$ is characterized by this second term. It can be expressed as the product of a 3×3 matrix $\mathbf{C}$, which consists of the second derivatives of the velocity field $\mathbf{u} = (u_1, u_2, u_3)$, and the infinitesimal displacement vector $\Delta\mathbf{x}$, such that

$\mathbf{C} \cdot \Delta\mathbf{x}$. (See Appendix for derivation details.) As an illustrative example where $\mathbf{C} \cdot \Delta\mathbf{x} \neq 0$, consider a two-dimensional domain containing a single point vortex. Assume the point vortex is placed at the origin and rotates counterclockwise with constant angular velocity, oriented upward normal to the xy-plane. Since this is a two-dimensional case, we have $u_3 = 0$, and the velocity gradients in the z-direction vanish for all components. Under this setting, only the components of $\mathbf{C}$ involving partial derivatives of u_1 and u_2 with respect to x or y remain; in particular, only the C_{31} and C_{32} components are nonzero, while all other components of $\mathbf{C}$ are zero. By the problem setup, the vorticity vector is given as $\boldsymbol{\omega} = (0, 0, \omega_z)$, where ω_z is assumed to follow an inverse radial profile such as $\omega_z(\mathbf{r}) = 1/r$, with $r = |\mathbf{r}|$ denoting the distance from the origin. Since this is a two-dimensional system, we write $\Delta\mathbf{x} = (\Delta x_1, \Delta x_2)$. After a few algebraic steps, we find

$$\begin{aligned}\mathbf{C} \cdot \Delta\mathbf{x} &= (\partial_x \omega_z)\Delta x_1 + (\partial_y \omega_z)\Delta x_2 \\ &= \nabla\omega_z \cdot \Delta\mathbf{x}.\end{aligned} \qquad (10)$$

Using $\omega_z = 1/r$, we obtain $\nabla\omega_z = -\mathbf{r}/|\mathbf{r}|^3$. Letting $\Delta\mathbf{x} = \mathbf{r}$, it follows that $\nabla\omega_z \cdot \Delta\mathbf{x} = -1/|\mathbf{r}| < 0$, which holds for all $\mathbf{r} \neq \mathbf{0}$. Figure 1 shows the plot of $\nabla\omega_z \cdot \Delta\mathbf{x}$, visually confirming that $\nabla\omega_z \cdot \Delta\mathbf{x}$ is always negative. Recall $\mathbf{\Omega} \equiv \boldsymbol{\omega}_0$. In summary, the expression $\mathbf{T}_a = \eta_r(\boldsymbol{\omega} - 2\boldsymbol{\omega}_0)$ is always nonzero in a two-dimensional point vortex system that contains only one point vortex.

Equation (2) gives the vorticity at position $\mathbf{r}$ as a convolution integral of the contributions from the surrounding subscale vortices; thus, we can evaluate the moments exerted by the surrounding vortices at position $\mathbf{r}$ by employing a multipole expansion of the right-hand side of Eq. (2) using the Legendre polynomials $P_n(x)$ as follows.

$$\begin{aligned}\overline{\boldsymbol{\omega}}(\mathbf{r}) &= \frac{1}{2C}\sum_{n=0}^{\infty}\frac{1}{r^{n+1}}\int r'^n P_n(\hat{\mathbf{r}} \cdot \hat{\mathbf{r}}')\boldsymbol{\omega}(\mathbf{r}')\, d\mathbf{r}' \\ &= \frac{1}{2Cr}\int\boldsymbol{\omega}(\mathbf{r}')d\mathbf{r}' + \\ &\quad \frac{1}{2Cr^3}\int\boldsymbol{\omega}(\mathbf{r}')(\mathbf{r}' \cdot \mathbf{r})d\mathbf{r}' + \cdots\end{aligned} \qquad (11)$$

The first term on the right-hand side represents the monopole term, which corresponds to the total sum of vorticity over the entire domain. In systems exhibiting dipole-like structures—where positive and negative vortices are paired—this term cancels out. In contrast, when all vortices within the domain rotate in the same direction, the contributions do not cancel, and the monopole term remains nonzero. The second term is the dipole term, which represents the first raw moment of vorticity over the domain. It characterizes the influence of spatial bias
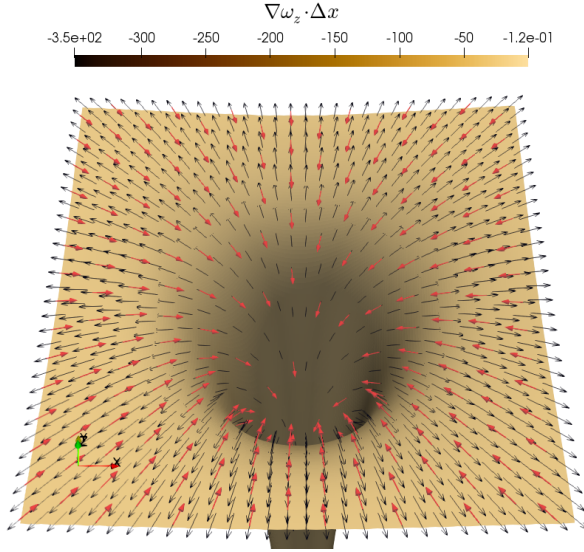
FIG. 1. A plot of $\nabla \omega_z \cdot \Delta \mathbf{x}$, visually confirming that $\nabla \omega_z \cdot \Delta \mathbf{x}$ is always negative for a stable vortex system with the vorticity distribution of $\omega_z(\mathbf{r}) = 1/r$. The red and gray colored arrows represent the vectors $\nabla \omega_z$ and $\Delta \mathbf{x}$, respectively.

in the vorticity distribution at position $\mathbf{r}$. For example, in a centrosymmetric configuration—where the vorticity is balanced in both horizontal and vertical directions—this term cancels and vanishes. Otherwise, it contributes a finite effect. Higher-order terms (from the third onward) represent finer features of the vorticity distribution, such as geometric deformation or biaxial asymmetry.

Taken together, $\boldsymbol{\omega} - 2\boldsymbol{\omega}_0$ is linearly proportional to the infinitesimal displacement vector and, therefore, is not negligible. In addition, $\boldsymbol{\omega} - 2\boldsymbol{\omega}_0$ can be nonzero in the vicinity of point vortices. The non-vanishing property of $\boldsymbol{\omega} - 2\boldsymbol{\omega}_0$, that is, $\exists\, \boldsymbol{\omega} - 2\boldsymbol{\omega}_0 \in \mathbb{R}, \quad \boldsymbol{\omega} - 2\boldsymbol{\omega}_0 \neq 0$, is one of the two necessary conditions required to ensure that Eq. (1) has physical significance. The other condition is the existence of a nonzero rotational viscosity: $\exists\, \nabla \times \boldsymbol{\omega} \in \mathbb{R}, \quad \nabla \times \boldsymbol{\omega} \neq 0$. Since interscale transfer is mediated by rotational viscosity $\nabla \times \boldsymbol{\omega}$, Eq. (3) would lose validity if the magnitude of $\nabla \times \boldsymbol{\omega}$ were identically zero. We take the rotation of Eq. (11) and examine the expansion of $\nabla \times \boldsymbol{\omega}$. A straightforward calculation reveals that the first-order term of $\nabla \times \boldsymbol{\omega}$ is given by

$$\nabla \times \boldsymbol{\omega}^{(1)} = -\frac{\mathbf{r}}{r^3} \times \boldsymbol{\Gamma}, \qquad (12)$$

where $\boldsymbol{\Gamma}$ is the integrated vorticity over the domain and is equal to the first term on the right-hand side of Eq. (11). Mathematically, for $\nabla \times \boldsymbol{\omega}^{(1)}$ to be nonzero at position $\mathbf{r}\ (\neq \mathbf{0})$, two conditions must be met: (i)

the vectors $\mathbf{r}$ and $\boldsymbol{\Gamma}$ must not be parallel, and (ii) the magnitude of $\boldsymbol{\Gamma}$ must not vanish. In 2D systems, the vorticity vector always points perpendicular to the xy-plane, so condition (i) is trivially satisfied. On the other hand, condition (ii) is satisfied in systems composed entirely of positive-signed vortices, as mentioned above. Thus, in such 2D systems, $\nabla \times \boldsymbol{\omega}^{(1)}$ is guaranteed to be nonzero.

In real systems, where point vortex models apply or in cases such as quantum vortices observed in a phase-controlled state—where vortex lines extend in the out-of-plane direction and rotate coherently—the nonzero nature of the first-order term can be expected to hold. In contrast, higher-order terms arise from asymmetries and deformations in vorticity distribution and may enhance or suppress the contribution from the first-order term, depending on the behavior of these higher-order structures.

Equation (3) illustrates that the transfer of vorticity across scales can occur recursively through the rotational viscosity term $\nabla \times \boldsymbol{\omega}$. The theoretical analysis in this section reveals that three conditions must be satisfied for this effect to emerge. First, the vorticity gradient ($\nabla \boldsymbol{\omega}$) must become sufficiently steep to yield a nonzero value of $\boldsymbol{\omega} - 2\boldsymbol{\omega}_0$, potentially resulting in non-solid-body rotational flows. Second, one of the following subconditions must hold: (i) the total vorticity over the domain is nonzero, and the higher-order moments of the vorticity distribution do not cancel its contribution; or (ii) the total vorticity is zero, while the moments of the vorticity distribution remain nonzero. Third, the attenuation effect introduced by filtering, represented by $\mathcal{F}$ (or $\mathcal{F} \cdot \mathcal{G}$), must be sufficiently small so as not to negate the preceding conditions. Viscous dissipation is expected to be the primary contributor to this attenuation. We have also shown that a system composed entirely of positively signed point vortices can simultaneously satisfy all three of these conditions. Moreover, the interscale transfer of vorticity can also be observed within the framework of the standard Navier–Stokes formulation. Equation (1) is mathematically equivalent to the conventional Navier–Stokes equations; its vorticity-explicit form does not alter the underlying dynamics. Therefore, in the following section, we investigate a freely decaying 2D turbulent flow in a finite domain initialized with a configuration of positive-signed point vortices. This analysis is conducted using the vorticity–streamfunction formulation of the Navier–Stokes equations for incompressible viscous fluids, in order to further explore the nature of the interscale transfer mechanism.

IV. SIMULATION OF FREELY DECAYING TURBULENCE

Problem setup.—We consider 2D vorticity transport in an incompressible viscous fluid confined to a square domain of size $[-L, L]^2$. The flow field is described using the vorticity–streamfunction formulation. As a preparatory step, the initial point vortex distribution used in the vorticity transport simulation is produced as follows. First, $N = 100$ positively signed point vortices, all with identical orientation, are randomly placed within a circular region of radius $R = L/2$ in the domain. Each vortex is assigned a nondimensional circulation strength of $\Gamma = 1$. To enforce the boundary condition on the circular edge, the method of image vortices is employed. We then computed the evolution of the vortices by calculating the interaction between each pair of vortices using the Biot-Savart law, and then integrated the results over time using the fifth-order Runge–Kutta–Fehlberg method [25]. All vortex-vortex interactions are directly calculated without approximation. We verify that the relative error in the total interaction energy remains within approximately 0.63% throughout the simulation.

The resulting velocity distribution is used as the initial condition of the vorticity–streamingfunction simulation by projecting it onto the square domain at the initial state. The simulation includes a preconditioning step to ensure a smooth transition at the boundaries. A Gaussian filter is applied in the region where the distance from the center exceeds $r > 0.8R$, gradually damping the velocity field toward the boundary. This outer region is treated as an absorbing layer, whereas no filtering is applied in the interior region $r < 0.8R$. The filtered velocity field on the boundary is fixed as the initial condition and remains unchanged during the simulation. The corresponding vorticity field is then recalculated from the velocity field. The parameter R is set to 1, which immediately yields $L = 2$. Thus, all lengths are nondimensionalized with respect to R. Taken together, the nondimensionalization is performed using R for length and Γ for circulation. Consequently, time and kinematic viscosity are also nondimensionalized as

$$\tilde{t} = \frac{\Gamma}{2\pi R^2} t, \quad \tilde{\nu} = \frac{2\pi}{\Gamma} \nu, \tag{13}$$

where t and ν are the dimensional time and kinematic viscosity, respectively.

Numerical conditions.—We conduct simulations of freely decaying 2D turbulence in a finite domain using three different values of the nondimensional kinematic viscosity: $\tilde{\nu} = 1.0 \times 10^{-2}$, 1.0×10^{-3}, and 1.0×10^{-4}. The square domain is discretized using a uniform Cartesian grid with resolution $(n_x, n_y) =$ $(2048, 2048)$, where n_x and n_y denote the number of grid points in each direction. The vorticity equation for incompressible flow is discretized in space using second-order central finite differences. For time integration, the fully implicit Crank–Nicolson scheme [26, 27] is adopted to achieve second-order temporal accuracy. The nonlinear advection term is evaluated at each time step using fixed-point iteration (Picard iteration). The velocity field is recovered as the perpendicular gradient of the streamfunction. The incompressibility constraint is enforced by solving the Poisson equation for the streamfunction (computed from vorticity) using the successive over-relaxation (SOR) method. The Red-Black algorithm [28] is implemented to ensure compatibility with parallel computation. The time step is initially set to $\Delta \tilde{t} = 1.0 \times 10^{-4}$ and adaptively adjusted to satisfy the Courant–Friedrichs–Lewy (CFL) condition based on the maximum velocity at each time step. A total of 6000 time steps were computed. Assuming physical parameters of circulation $\Gamma = 1.0 \times 10^{-3}$ cm²/s and radius $R = 1.0$ cm, this corresponds to approximately 3770 seconds (about 1 hour and 3 minutes) of physical time under freely decaying conditions.

Results.—The three enlarged panels at the top of Fig. 2 show the vorticity distributions at the nondimensionalized time $\tilde{t} = 0.6$ for three different viscosity conditions: (a) $\tilde{\nu} = 1.0 \times 10^{-2}$, (b) 1.0×10^{-3}, and (c) 1.0×10^{-4}, respectively. The vorticity is plotted on a logarithmic scale, and the absorbing region is omitted for clarity. Below each of these panels, snapshots of the velocity and vorticity distributions from the initial state to the final simulation step are provided for reference. The velocity distribution is shown on the left, and the vorticity distribution on the right. The views at the bottom right of each snapshot correspond to the magnified panels at the top of Fig. 2.

Figure 2 clearly illustrates the dependence of the vorticity structure on viscosity. Interpreting the figure as a table, the second row corresponds to the distribution observed immediately after the simulation start. At this stage, no clear differences in the vorticity distribution are observed across the different viscosities. However, the subsequent evolution diverges markedly between (a) through (c). In panel (c), where the viscosity is lowest, the influence of the initial condition persists even after long time evolution, with many small-scale vortices remaining visible. In contrast, in panel (b), with ten times higher viscosity, the vortices have grown larger and fewer in number. In panel (a), where the viscosity is 100 times higher than (c), a single large vortex spanning the entire domain is observed in the final state. These results are physically consistent. According to tur-

bulence theory, viscous effects scale with the square of the wavenumber, so as viscosity increases, high-wavenumber (small-scale) vortices dissipate preferentially, leaving low-wavenumber (large-scale) structures dominant.

The persistence of the initial point-vortex-like structure in panel (c) holds significant scientific importance. In the previous section, three necessary conditions for interscale vorticity transfer via Eq. (3) were proposed. A freely decaying system consisting solely of positive-sign point vortices is expected to meet these conditions, as the steep gradient of vorticity (first condition) and nonzero total circulation (the first half of condition (ii)) are both inherently satisfied. Although the exact contribution of the vorticity moments is unknown, it is physically improbable that their sum would exactly cancel out the total circulation under asymmetric arrangements. Consequently, it is reasonable to consider that two out of the three conditions are effectively satisfied. The uncertainty lies in the third condition: the magnitude of viscous dissipation that inhibits interscale transfer. Figure 2 presents the simulation results used to evaluate this third condition under viscosities ranging from 1.0×10^{-2} to 1.0×10^{-4}. The clear retention of small-scale structures in panel (c) suggests that as viscosity decreases from (a) to (c), dissipation becomes sufficiently small to no longer obstruct the interscale transfer described by Eq. (3).

V. SPECTRAL ANALYSIS OF ROTATIONAL VISCOSITY

Spectral analyses were conducted for three quantities based on the results shown in Fig. 2: energy E, rotational viscosity $|\nabla \times \boldsymbol{\omega}|^2$, and enstrophy $|\boldsymbol{\omega}|^2$. In an isolated, freely decaying system without external forcing, the intensity of these quantities naturally decreases over time. Figure 3 presents the spectral evolution: (a)–(c) in the top row for energy E, (d)–(f) in the middle row for rotational viscosity $|\nabla \times \boldsymbol{\omega}|^2$, and (g)–(i) in the bottom row for enstrophy $|\boldsymbol{\omega}|^2$. In each plot, the blue line represents the spectrum shortly after the onset of decay, and yellow lines show the spectra at the final time $\tilde{t} = 0.6$. In each row, the left panel corresponds to the high viscosity ($\tilde{\nu} = 1.0 \times 10^{-2}$), the center to medium viscosity ($\tilde{\nu} = 1.0 \times 10^{-3}$), and the right to low viscosity ($\tilde{\nu} = 1.0 \times 10^{-4}$), respectively. In the energy spectra (a)–(c), the trends observed in Fig. 2 are confirmed: at high viscosity, small-scale (high-wavenumber) components dissipate rapidly, resulting in dominance by large-scale (low-wavenumber) structures. In the enstrophy spectra (g)–(i), an opposite trend is observed: the recovery of high-frequency components—

previously decayed over time—becomes progressively pronounced with increasing viscosity. This reflects a shift of spectral intensity toward higher wavenumbers in contrast to energy spectra, consistent with an inverse cascade in energy and a direct cascade in enstrophy. The downward shift in spectral intensity over time is also reasonable, given the dissipative nature of the system. These spectral results support the reliability of the simulations, as the typical features of 2D turbulence—energy accumulation at large scales and enstrophy transfer to small scales—are well reproduced.

A particularly notable result appears in the rotational viscosity spectra (d)–(f). Due to the presence of localized vortices, a peaked spectral shape appears at high wavenumbers, with a noticeable dip separating it from the low-wavenumber region. This dip is marked with red downward arrows in the plots. Interestingly, this characteristic shape shifts toward lower wavenumbers over time in all cases, while maintaining its overall shape. That is, the initially small-scale feature in $|\nabla \times \boldsymbol{\omega}|$ transfers to larger scales as time progresses. In the high- and medium-viscosity cases (Figs. 3(d) and (e)), this transfer is overwhelmed by dissipation, and the characteristic spectral shape does not persist into the final state. In contrast, in the low-viscosity case (Fig. 3(f)), the upward red arrow indicates that the dip in the spectrum—first observed at early stages—remains visible even at later times (orange line). This supports the conclusion that interscale transfer of $\nabla \times \omega$ has occurred. It is also noted that the temporary disturbance in the upper-right corner of Fig. 3(f) results from transient spectral redistribution occurring between $\tilde{t} = 0.015$ and $\tilde{t} = 0.05$. In summary, the simulation of freely decaying 2D turbulence initiated from a system of positive-signed point vortices reproduces the scale-to-scale transfer of rotational viscosity explicitly expressed in Eq. (3).

In this study, we demonstrated that initializing the system with a point vortex distribution exhibiting locally concentrated circulation results in a rotational viscosity spectrum $|\nabla \times \boldsymbol{\omega}|^2$ characterized by a distinct dip in a specific wavenumber band. As the system evolves in time, this spectral distribution is observed to shift toward lower frequencies while maintaining its overall shape. This behavior indicates that small-scale ordered structures are transferred to larger scales via the rotational viscosity term.

To provide a qualitative understanding of why this transfer occurs through the rotational viscosity $|\nabla \times \boldsymbol{\omega}|$ rather than through a conserved quantity, we consider the Taylor expansion of the velocity field as in Eq. (8) and its rotational form in Eq. (9). When the curl of Eq. (8) is taken to derive Eq. (9), the degree of dependence on the displacement $\Delta \mathbf{x}$ is

reduced, and $\nabla \times \mathbf{u}$ becomes linearly proportional to $\Delta \mathbf{x}$. Since $\nabla \times \boldsymbol{\omega}$ is derived by applying an additional curl to both sides of Eq. (9), the order of $\Delta \mathbf{x}$ in each term of the expansion is reduced by one further order. As a result, $\nabla \times \boldsymbol{\omega}$ consists of a constant vector evaluated at $\mathbf{x}_0$ and higher-order terms proportional to $\Delta \mathbf{x}^2$ and beyond. Neglecting these higher-order terms, $\nabla \times \boldsymbol{\omega}$ can be approximated by a constant vector evaluated at $\mathbf{x}_0$ alone. Taken together, this implies that within a small neighborhood around $\mathbf{x}_0$, $\nabla \times \boldsymbol{\omega}$ acts as a uniform rotational viscous force applied to the surrounding region, regardless of proximity to $\mathbf{x}_0$ within that neighborhood.

An important point to note here is that, the notion of "neighborhood" in this context is somewhat relative, as it depends on the choice of characteristic length scale in the dynamical system. However, in the present case, the interpretation is straightforward. The "neighborhood" associated with the rotational viscosity field can be interpreted as follows. In mathematics, it is known that the radius of convergence of a Taylor expansion corresponds to the distance from the expansion point $\mathbf{x}_0$ to the nearest singularity [29]. When the system is approximated by localized vortices with concentrated circulation (i.e., point vortices), this nearest singularity may reasonably be interpreted as the distance to the closest vortex core from $\mathbf{x}_0$. Therefore, in regions where the vortex distribution is sparse rather than densely packed, the rotational viscous force may be regarded as a form of nonlocal or long-range interaction.

Consider now a scenario where a vortex $\mathbf{A}$ is located at position $\mathbf{x}_0$, and two other vortices $\mathbf{B}$ and $\mathbf{C}$ are located in its vicinity. As discussed above, in the neighborhood of $\mathbf{x}_0$, $\nabla \times \boldsymbol{\omega}$ can be treated as a constant vector. Thus, the viscous interaction strength exerted by vortex $\mathbf{A}$ on both $\mathbf{B}$ and $\mathbf{C}$ can be regarded as independent of their distances from $\mathbf{A}$. Figure 4 presents the logarithmic-scale distributions of the vorticity norm $|\boldsymbol{\omega}|$ (left) and the rotational vorticity norm $|\nabla \times \boldsymbol{\omega}|$ (right) at the final simulation state under $\tilde{\nu} = 1.0 \times 10^{-4}$. In Fig. 4(a), the region between two vortices appears dark, which may initially suggest a lack of correlation between them. However, Fig. 4(b) reveals that a rotational viscosity $|\nabla \times \boldsymbol{\omega}|$ is indeed present in these regions, indicating interaction.

In summary, this analysis provides a qualitative understanding that vortices interact through the long-range rotational viscous force induced by $\nabla \times \boldsymbol{\omega}$. This highlights $\nabla \times \boldsymbol{\omega}$ as a key factor in the formation of ordered structures.

VI. CONCLUSION

Rotational viscosity ($\nabla \times \boldsymbol{\omega}$) is not typically emphasized in turbulence studies, which often focus on conserved quantities such as energy and enstrophy. However, we have shown that initializing the system with a point vortex distribution featuring locally concentrated circulation leads to a rotational viscosity spectrum exhibiting a distinct dip in a specific wavenumber range. This structure persists over time while shifting toward lower frequencies, suggesting that small-scale ordered structures are transmitted to larger scales via the rotational viscosity term. To the best of the author's knowledge, this represents the first numerical observation of such behavior. Previous theoretical work predicted recursive interscale transfer of rotational viscosity within the spin angular momentum-conserving Navier–Stokes model, but lacked numerical verification. In addition, the underlying assumption—the existence of local non-solid rotational flows—had not been theoretically justified.

This study addressed both issues. The model was reinterpreted within the turbulence hierarchy framework: small-scale vortices may appear non-solid from a local perspective, yet still appear solid from a large-scale viewpoint. Based on continuum mechanics and vector analysis, we showed that the deviation $\boldsymbol{\omega} - 2\boldsymbol{\omega}_0$ is linearly proportional to first-order spatial variation, and thus non-negligible. These findings support the theoretical validity of the spin-conserving Navier–Stokes equations and suggest that, under certain conditions, small-scale order can be transmitted to large scales via $\nabla \times \boldsymbol{\omega}$. Spectral analysis of freely decaying two-dimensional turbulence confirms this transfer mechanism through the observed downward shift in $|\nabla \times \boldsymbol{\omega}|^2$ spectra over time.

Appendix A: Derivation of the second term in Equation (9)

The i-th component of the curl of vector $\mathbf{u}$ is expressed using the Levi-Civita symbol as follows:

$$(\nabla \times \mathbf{u})_i = \varepsilon_{inm} \frac{\partial u_m}{\partial x_n}, \qquad (A1)$$

where u_m represents the mth component of velocity $\mathbf{u}$. Denote the kth-order term in the Taylor series of u_m as $u_m^{(k)}$ ($k = 1, 2, 3$). The third term on the right-hand side of Eq. (8) can be rewritten using the

right-hand side of Eq. (A1) as follows:

$$
\begin{aligned}
(\nabla \times \mathbf{u})_i^{(2)} &= \varepsilon_{inm} \frac{\partial u_m^{(2)}}{\partial x_n} \\
&= \varepsilon_{inm} \frac{\partial}{\partial x_n} \left[\frac{1}{2} \frac{\partial^2 u_m}{\partial x_j \partial x_k} \Delta x_j \Delta x_k \right] \\
&= \varepsilon_{inm} \frac{1}{2} \frac{\partial^2 u_m}{\partial x_j \partial x_k} [\delta_{nj} \Delta x_k + \Delta x_j \delta_{nk}] \\
&= \varepsilon_{inm} \frac{1}{2} \left[\frac{\partial^2 u_m}{\partial x_n \partial x_k} \Delta x_k + \frac{\partial^2 u_m}{\partial x_j \partial x_n} \Delta x_j \right] \\
&= \varepsilon_{inm} \frac{\partial^2 u_m}{\partial x_j \partial x_n} \Delta x_j \\
&= C_{ij} \Delta x_j. \tag{A2}
\end{aligned}
$$

Here, interchange of partial derivatives is allowed due to the assumption of sufficient smoothness of the velocity field. C_{ij} is a 3×3 matrix composed of the second-order derivatives of velocity, expressed as follows:

$$
\mathbf{C} := \begin{bmatrix} \partial_{12} u_3 - \partial_{13} u_2 & \partial_{22} u_3 - \partial_{23} u_2 & \partial_{32} u_3 - \partial_{33} u_2 \\ \partial_{13} u_1 - \partial_{11} u_3 & \partial_{23} u_1 - \partial_{21} u_3 & \partial_{33} u_1 - \partial_{31} u_3 \\ \partial_{11} u_2 - \partial_{12} u_1 & \partial_{21} u_2 - \partial_{22} u_1 & \partial_{31} u_2 - \partial_{32} u_1 \end{bmatrix}
\tag{A3}
$$

DATA AVAILABILITY STATEMENT

No new data were created or analyzed in this study.

[1] L. Onsager, Statistical hydrodynamics, Il Nuovo Cimento (Supplemento) **6**, 279 (1949).

[2] R. H. Kraichnan, Inertial ranges in two-dimensional turbulence, Physics of Fluids **10**, 1417 (1967).

[3] U. Frisch, *Turbulence: The Legacy of A. N. Kolmogorov* (Cambridge University Press, 1995).

[4] P. A. Davidson, *Turbulence: An Introduction for Scientists and Engineers*, 2nd ed. (Oxford University Press, 2015).

[5] R. J. Donnelly, *Quantized Vortices in Helium II* (Cambridge University Press, 1991).

[6] C. F. Barenghi, L. Skrbek, and K. R. Sreenivasan, Introduction to quantum turbulence, Proceedings of the National Academy of Sciences **111**, 4647 (2014).

[7] D. W. Condiff and J. S. Dahler, Fluid mechanical aspects of antisymmetric stress, The Physics of Fluids **7**, 842 (1964).

[8] A. C. Eringen, Theory of micropolar fluids, Journal of Mathematics and Mechanics **16**, 1 (1966).

[9] F. Peters, L. Lobry, and E. Lemaire, Pressure-driven flow of a micro-polar fluid: Measurement of the velocity profile, Journal of Rheology **54**, 311 (2010).

[10] P. Ilg, Multiparticle collision dynamics for ferrofluids, The Journal of Chemical Physics **156**, 144905 (2022).

[11] S. Tsuzuki, Multi-scale physics of cryogenic liquid helium-4: Inverse coarse-graining properties of smoothed particle hydrodynamics, arXiv preprint arXiv:2501.14244 (2025).

[12] G. KAWAHARA, S. KIDA, M. TANAKA, and S. YANASE, Wrap, tilt and stretch of vorticity lines around a strong thin straight vortex tube in a simple shear flow, Journal of Fluid Mechanics **353**, 115–162 (1997).

[13] S. Tsuzuki, A hydrodynamic approach to reproduce multiple spinning vortices in horizontally rotating three-dimensional liquid helium-4, Physics of Fluids **36**, 087155 (2024).

[14] G. K. Batchelor, *An introduction to fluid dynamics* (Cambridge university press, 2000).

[15] A. Bennett, *Lagrangian fluid dynamics* (Cambridge University Press, 2006).

[16] S. Haeri and J. Shrimpton, A mesoscopic description of polydispersed particle laden turbulent flows, Progress in Energy and Combustion Science **37**, 716 (2011).

[17] P. J. Hoogerbrugge and J. M. V. A. Koelman, Simulating microscopic hydrodynamic phenomena with dissipative particle dynamics, Europhysics Letters **19**, 155 (1992).

[18] J. M. V. A. Koelman and P. J. Hoogerbrugge, Dynamic simulations of hard-sphere suspensions under steady shear, Europhysics Letters **21**, 363 (1993).

[19] K. Muller, D. A. Fedosov, and G. Gompper, Smoothed dissipative particle dynamics with angular momentum conservation, Journal of Computational Physics **281**, 301 (2015).

[20] P. Español, Fluid particle model, Phys. Rev. E **57**, 2930 (1998).

[21] P. Español, M. Serrano, and I. Zuñiga, Coarse-graining of a fluid and its relation with dissipative particle dynamics and smoothed particle dynamic, International Journal of Modern Physics C **08**, 899 (1997).

[22] W. Dzwinel, D. A. Yuen, and K. Boryczko, Bridging diverse physical scales with the discrete-particle paradigm in modeling colloidal dynamics with mesoscopic features, Chemical Engineering Science **61**, 2169 (2006), Papers Presented at the Eleventh and Twelfth Nisshin Engineering Particle Technology International Symposium.

[23] M. Tsubota, M. Kobayashi, and H. Takeuchi, Quantum hydrodynamics, Physics Reports **522**, 191 (2013), Quantum hydrodynamics.

[24] L. Galantucci, A. W. Baggaley, C. F. Barenghi, and G. Krstulovic, A new self-consistent approach of quantum turbulence in superfluid helium, The European Physical Journal Plus **135**, 547 (2020).

[25] E. Fehlberg, Klassische runge-kutta-formeln funfter und siebenter ordnung mit schrittweiten-kontrolle, Computing **4**, 93 (1969).

[26] J. Crank and P. Nicolson, A practical method for numerical evaluation of solutions of partial differential equations of the heat-conduction type, Mathematical Proceedings of the Cambridge Philosophical Society **43**, 50 (1947).

[27] J. G. Heywood and R. Rannacher, Finite-element approximation of the nonstationary navier–stokes problem. part iv: Error analysis for second-order time discretization, SIAM Journal on Numerical Analysis **27**, 353 (1990).

[28] L. ADAMS and J. ORTEGA, A multi-color sor methodfor parallel computation, ICASE report (1982).

[29] S. Christiansen and P. A. Madsen, On truncated taylor series and the position of their spurious zeros, Applied Numerical Mathematics **56**, 91 (2006).
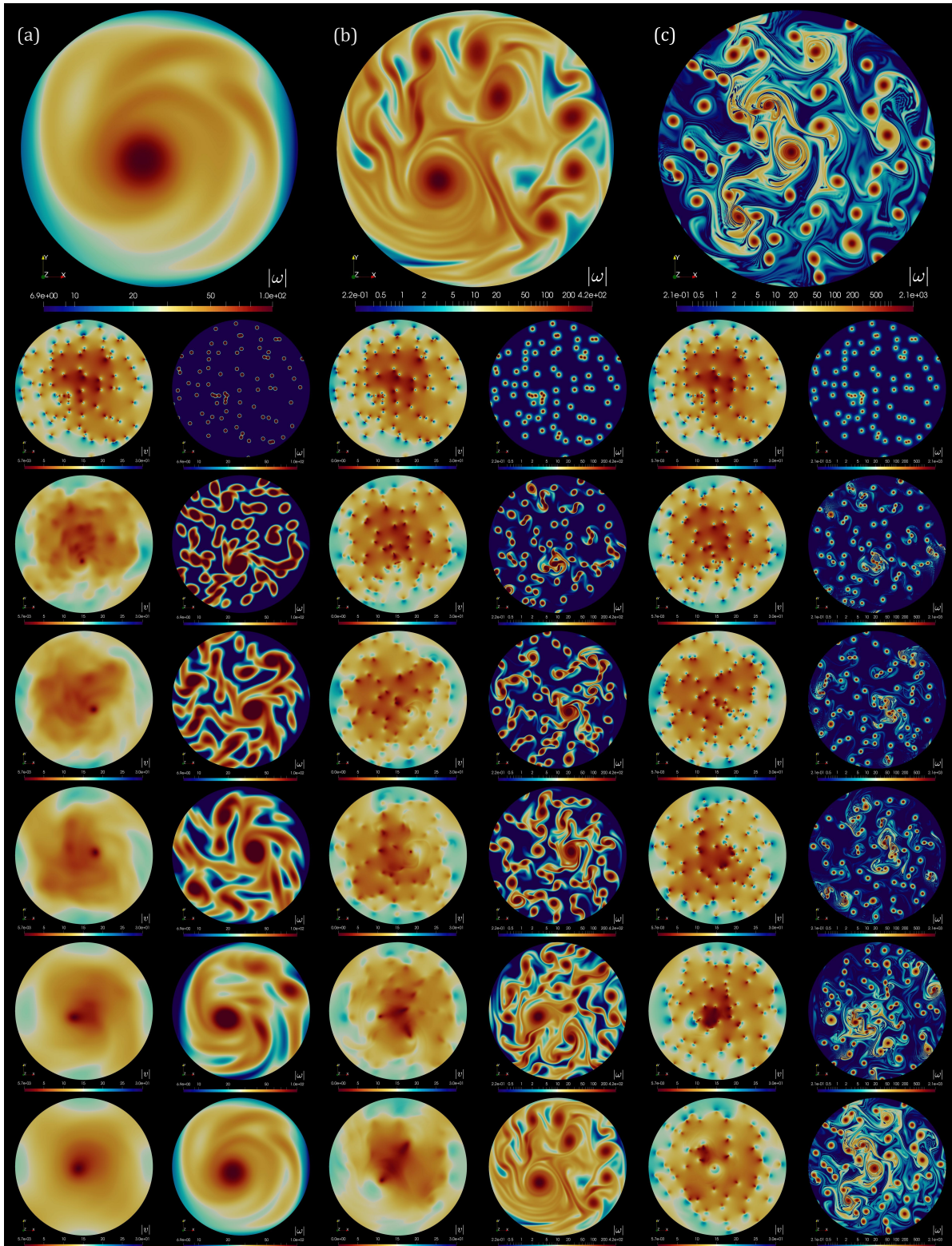
FIG. 2. Snapshots of the numerical simulations for a freely decaying two-dimensional turbulent flow using the vorticity-streamfunction formulation of the Navier-Stokes equations for incompressible viscous fluids. The flow was initialized with a configuration of positively signed point vortices. The top three panels are enlarged views of the vorticity distributions at a nondimensionalized time $\tilde{t} = 0.6$ for three different viscosity conditions: (a) $\tilde{\nu} = 1.0 \times 10^{-2}$, (b) 1.0×10^{-3}, and (c) 1.0×10^{-4}, respectively. Below each of these panels are snapshots of the velocity and vorticity distributions from the initial state to the final simulation step. The velocity distribution is shown on the left, and the vorticity distribution is shown on the right.
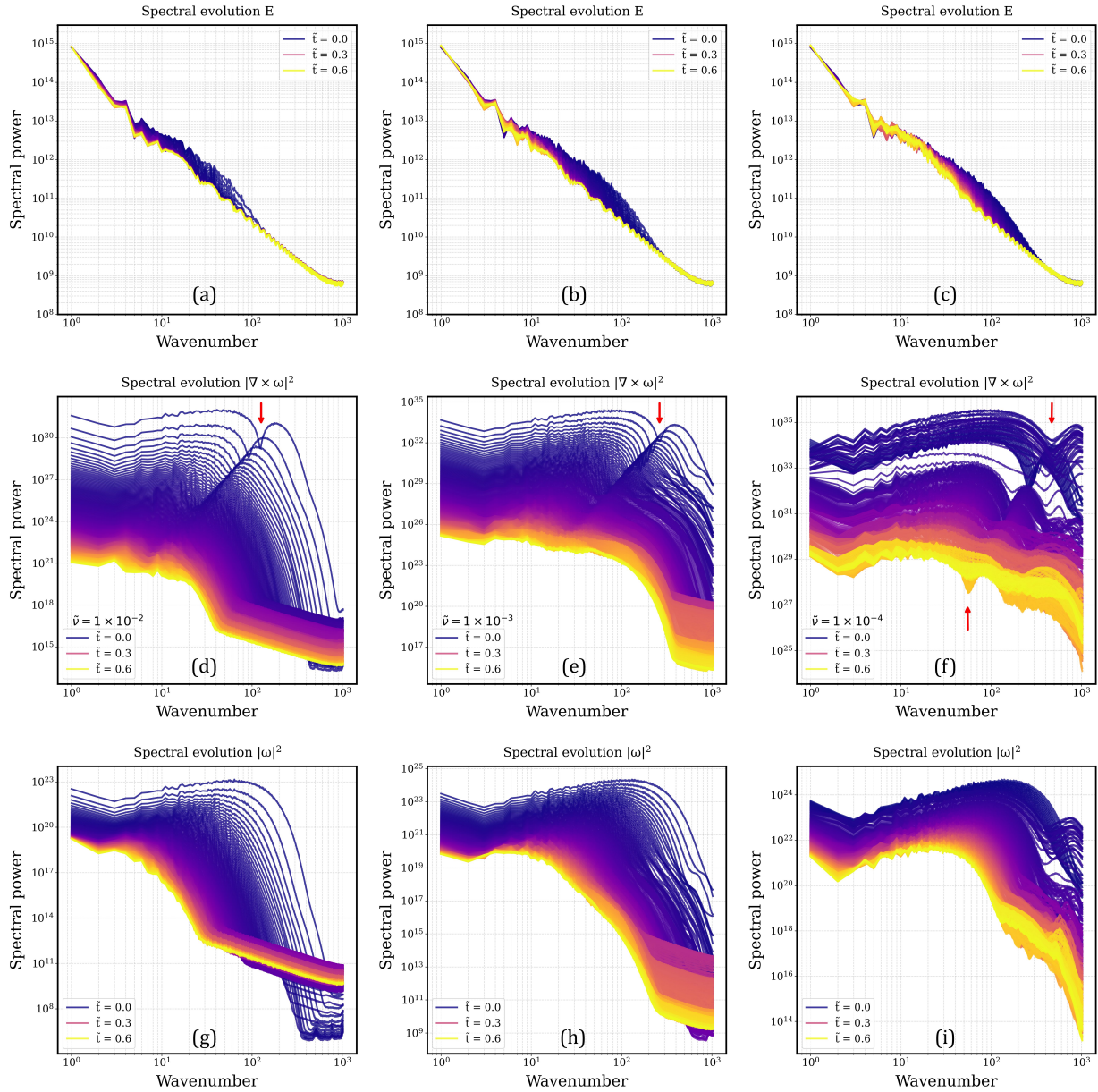
FIG. 3. Results of the spectral analyses conducted for three different quantities: energy E, rotational vorticity $|\nabla \times \boldsymbol{\omega}|^2$, and enstrophy $|\boldsymbol{\omega}|^2$. Panels (a) through (c) in the top row display the spectral evolution of E. Panels (d) through (f) in the middle row show the spectral evolution of $|\nabla \times \boldsymbol{\omega}|^2$. Panels (g) through (i) in the bottom row depict the spectral evolution of $|\boldsymbol{\omega}|^2$. The blue lines represent the spectra at the onset of decay, while the yellow lines represent the spectra at the final time $\tilde{t} = 0.6$. Each row is divided into three panels, corresponding to different levels of viscosity: high viscosity ($\tilde{\nu} = 1.0 \times 10^{-2}$) in the left panel, medium viscosity ($\tilde{\nu} = 1.0 \times 10^{-3}$) in the middle panel, and low viscosity ($\tilde{\nu} = 1.0 \times 10^{-4}$) in the right panel.
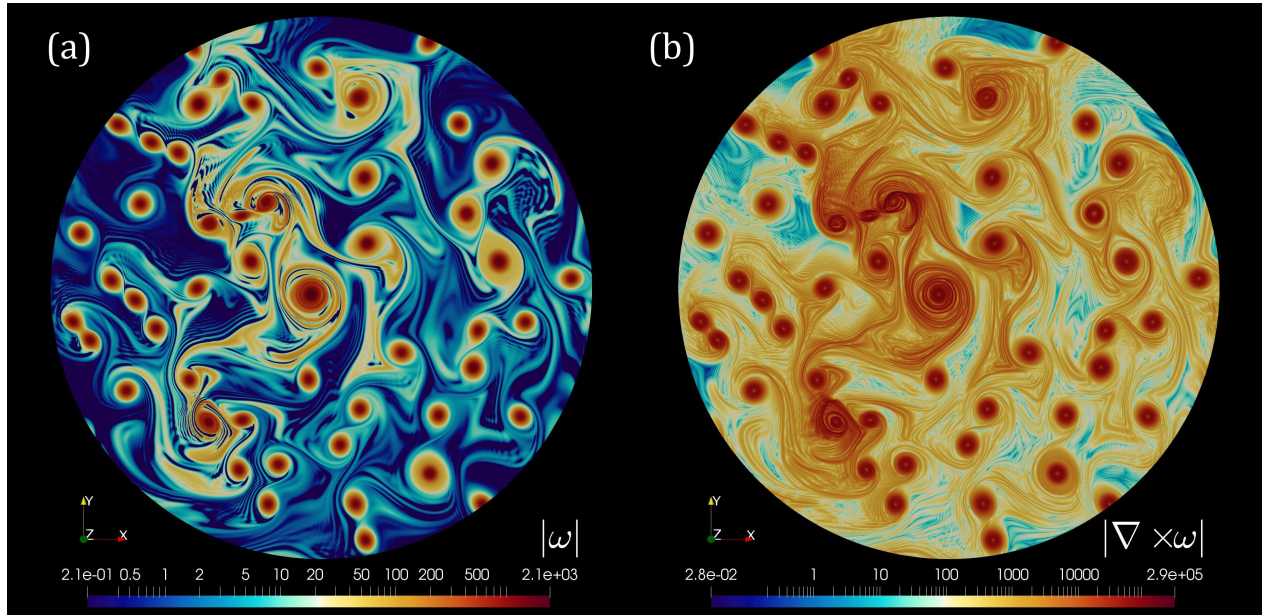
FIG. 4. Distributions of the vorticity norm $|\boldsymbol{\omega}|$ (left) and the rotational vorticity norm $|\nabla \times \boldsymbol{\omega}|$ (right) at the final simulation state under $\tilde{\nu} = 1.0 \times 10^{-4}$. In (a), there are the region between two vortices appears dark, apparently suggesting a lack of strong correlation between them. However, the right panel reveals that a rotational viscous field $|\nabla \times \boldsymbol{\omega}|$ is indeed present in these regions, indicating interaction.